

# Three-dimensional bond-order instability in infinite-layer nickelates due to nonlocal quantum interference

Seiichiro Onari and Hiroshi Kontani

*Department of Physics, Nagoya University, Furo-cho, Nagoya 464-8602, Japan.*

(Dated: December 15, 2023)

Recently discovered superconducting infinite-layer nickelates  $R\text{NiO}_2$  ( $R=\text{Nd, La, Pr}$ ) attracts increasing attention as a similar system to cuprates. Both  $R\text{NiO}_2$  and YBCO cuprates display the three-dimensional (3D) CDW with wave vector  $\mathbf{q} \sim (2\pi/3, 0, q_z)$ , while  $q_z$  is non-zero and incommensurate in the former system. Here, we reveal that the characteristic CDW in  $R\text{NiO}_2$  can be explained as the quantum interference between paramagnons, by focusing on the following characteristics of  $R\text{NiO}_2$ : (i) prominent three-dimensionality in the Fermi surface and (ii) large self-hole-doping ( $\sim 14\%$ ). This mechanism predicts the emergence of the  $d_{x^2-y^2}$ -wave bond order at a secondary 3D nesting vector  $\mathbf{q}^c \sim (2\pi/3, 0, q_z^c)$  ( $q_z^c = 0.2\pi \sim 2\pi/3$ ). The obtained strong bond fluctuations lead to the non-Fermi liquid electronic states and superconducting states in nickelates.

The recent discovery of superconducting infinite-layer nickelates with similar electronic structures and phase diagrams to cuprates has stimulated much attention [1–3]. In fact, infinite-layer nickelates  $R\text{NiO}_2$  ( $R=\text{Nd, La, Pr}$ ) have Ni- $3d^9$  configuration, which is the same as Cu- $3d^9$  in cuprates. A high superconducting transition temperature  $T_{\text{SC}} \lesssim 30\text{K}$  has been reported in  $R\text{NiO}_2$  [4], which may be due to the electron structure similar to cuprates.

However, there are many differences between  $R\text{NiO}_2$  and cuprates. The charge-transfer energy estimated by experiments and theories in  $R\text{NiO}_2$  is larger than cuprates [5–10]. Thus,  $R\text{NiO}_2$  is close to the Mott-Hubbard regime, away from the charge-transfer regime in Zaanen-Sawatzky-Allen classification [11]. Significant differences from cuprates are (i) prominent three-dimensionality in the Fermi surface (FS) and (ii) large self-hole-doping. As for (i), the FS composed of Ni  $d_{x^2-y^2}$  orbital in  $\text{NdNiO}_2$  has three-dimensionality, while cuprates have two-dimensional (2D) FS. As for (ii), self-hole-doping ( $p_{\text{self}} \sim 0.14$ ) for Ni  $d_{x^2-y^2}$  orbital in  $\text{NdNiO}_2$  is induced since the FSs of the Nd orbitals emerge [6, 7]. We define an effective hole-doping  $p_{\text{eff}} = x + p_{\text{self}}$  in  $\text{Nd}_{1-x}\text{Sr}_x\text{NiO}_2$  to make direct comparison with  $p_{\text{eff}} = x$  in cuprates without the self-hole-doping.

Very recently, a three-dimensional (3D) CDW at wave vector  $\mathbf{q} = (q_x, 0, q_z)$  ( $q_x \sim 2\pi/3, q_z \neq 0$ ) has been observed by RIXS measurements in  $R_{1-x}\text{Sr}_x\text{NiO}_2$  [12–15]. The value of  $q_x \sim 2\pi/3$  corresponds to the period-three CDW in the  $x$ -direction. The value of  $q_x$  and the CDW transition temperature ( $T_c^{\text{RIXS}}$ ) observed by RIXS measurements decrease with  $p_{\text{eff}}$ . Schematic  $p_{\text{eff}}$  dependences of  $T_c^{\text{RIXS}}$  observed in nickelates and overdoped cuprates are shown in Supplementary Material (SM) A [16].  $T_c^{\text{RIXS}} \lesssim 400\text{K}$  in nickelates is higher than  $T_c^{\text{RIXS}} \lesssim 200\text{K}$  in cuprates. In both systems, the CDW quantum critical point (QCP) attracts great attention since  $T_{\text{SC}}$  becomes the maximum around the CDW QCP. In nickelates, critical hole-doping is  $p_c^{\text{eff}} \sim 0.25$  [12], while  $p_c^{\text{eff}} \sim 0.18$  in YBCO cuprates [17, 18]. Near the CDW QCP, the non-Fermi-liquid transport phenomena

have been observed [19–22]. Interestingly, the pseudogap observed in  $\text{Bi2212}$  for  $p_{\text{eff}} < 0.19$  [23, 24] would originate from the CDW formation. In contrast, Ref. [25] reports the absence of the CDW in electron-doped cuprates.

The electronic states in  $R\text{NiO}_2$  have been actively studied by using the dynamical mean-field theory (DMFT) [26, 27]. Beside the DMFT, the pair-density-wave [28–30], intertwined-order [28, 31], spin-nematic/vestigial-order [32–38], and orbital/bond-order [39–57] scenarios have been proposed to explain the CDW. According to Refs. [54–56, 58], the bond order and spin current order in cuprates can be explained by “the paramagnon-interference mechanism” described by the non-local vertex corrections. The similar theory has been applied to Fe-based superconductors [43–48], twisted bilayer graphene [59] and kagome metal [60, 61].

In this paper, we study the origin of the 3D CDW in  $R\text{NiO}_2$  based on the paramagnon-interference mechanism by using the 3D density-wave (DW) equation. We find that the 3D bond order with wave vector  $\mathbf{q}^c = (2\pi/3, 0, q_z^c)$  ( $0.2\pi \lesssim q_z^c \lesssim 2\pi/3$ ) emerges, which is consistent with the 3D CDW with  $q_z \sim 0.6\pi$  and  $q_z \lesssim 0.54\pi$  observed in experiments [14]. The obtained  $p_{\text{eff}}$  dependences of the bond order are consistent with experiments [12]. The obtained strong bond fluctuations lead to the non-Fermi liquid states and superconducting states [60].

The 3D bond order is derived by the paramagnon interference due to the Aslamazov–Larkin (AL) terms in Fig.1(a), which are non-local irreducible vertex corrections. In the paramagnon-interference mechanism, the charge channel order with  $\mathbf{q} = \mathbf{Q} - \mathbf{Q}'$  originates from the interference between the spin fluctuation with  $\mathbf{q} = \mathbf{Q}$  and that with  $\mathbf{q} = \mathbf{Q}'$ . This mechanism is not derived from the mean-field-like approximation, such as the random-phase-approximation (RPA) and the fluctuation-exchange approximation without the vertex corrections. The present paramagnon-interference mechanism would be a key concept toward a unified understanding of the CDW orders in nickelates and cuprates.

We analyze the following 3D three-orbital Hubbard

model for NdNiO<sub>2</sub>, where  $d_{x^2-y^2}$  orbital of Ni,  $d_{z^2}$  and  $d_{xy}$  orbitals of Nd are taken into account:  $H = H^0 + H^U$ , where  $H^0$  is the tight-binding model for NdNiO<sub>2</sub> based on Ref. [8]. We introduce the next-nearest-interlayer hopping  $t_{z2}$  of Ni  $d_{x^2-y^2}$  orbital in order to reproduce the parallel FSs around the M point obtained by other first-principles calculations [9, 10]. Details of the model are explained in SM A [16]. The orbitals 1, 2, and 3 denote Ni  $d_{x^2-y^2}$  orbital, Nd  $d_{z^2}$  orbital, and Nd  $d_{xy}$  orbital, respectively.  $H_U$  is the Coulomb interaction, where the Coulomb interaction of only orbital 1 is taken into account since the results including the Coulomb interactions of the three orbitals are almost the same.

Figures 1(b) and S1(a) in SM A [16] show 3D FSs and band dispersion in this model ( $x = 0$ ), where the number of electrons is 1. Since the FSs composed of orbitals 2 and 3 appear, the number of electrons for the Ni  $d_{x^2-y^2}$  orbital is about 0.86 (self-hole-doping  $p_{\text{self}} = 0.14$ ), which is consistent with the self-hole-doping reported in Ref. [6, 7]. In Nd<sub>1-x</sub>Sr<sub>x</sub>NiO<sub>2</sub>, the value of  $p_{\text{self}}$  decreases with doping  $x$ , and  $p_{\text{self}} \sim 0.09$  for  $x = 0.15$ .

Here, we discuss the FS of the Ni  $d_{x^2-y^2}$  orbital, which is important to realize the CDW. Figure 1(c) shows the FSs in  $k_z = 0$  plane, where the FS composed of Ni  $d_{x^2-y^2}$  orbital is similar to the FS of YBCO cuprates. Figure 1(d) shows the FSs and 3D nesting  $\mathbf{q}^c \sim (2\pi/3, 0, q_z^c)$  around X point. The spin susceptibility at  $\mathbf{q}^c$  is smaller than that at primary nesting  $\mathbf{Q}_s$ . The nesting  $\mathbf{q}^c$  at the FS around R point shown in Fig. 1(e), which is absent in cuprates, assists the secondary nesting. The small instability by the secondary nesting causes the bond order at  $\mathbf{q} = \mathbf{q}^c$  ( $0.2\pi \lesssim q_z^c \lesssim 2\pi/3$ ) with the aid of the AL vertex correction in the present theory as shown later.

Before discussing the CDW order, we calculate the spin susceptibility for orbital 1  $\chi^s(\mathbf{q})$  because we discuss the spin-fluctuation-driven CDW mechanism. We obtain  $\chi^s(\mathbf{q})$  for  $\mathbf{q} = (\mathbf{q}, \omega_m = 2m\pi T)$  based on the RPA, which is introduced in SM A [16].  $\chi^s(\mathbf{q}) \propto (1 - \alpha_s)^{-1}$ , where  $\alpha_s$  is the spin Stoner factor.  $\alpha_s = 1$  corresponds to spin-ordered state. Hereafter, we fix  $T = 60\text{meV} \sim 700\text{K}$  using  $k_B = 1$  unless otherwise noted.

Figures 2(a) and (b) show the obtained spin susceptibility for orbital 1  $\chi^s(\mathbf{q}, 0)$ , which has rather broad peak around  $\mathbf{Q}_s = (2\pi/3, 2\pi/3, \pi)$ . The value of  $\chi^s(\mathbf{q}, 0)$  becomes small away from the  $q_z = \pi$  plane, and other orbital components of spin susceptibility are very small. In the present study, we set the Coulomb interaction  $U_1 = 1.43\text{eV}$  for the orbital 1, which is smaller than  $U_1 = 3\text{-}4\text{eV}$  obtained by the first-principles calculations [6, 9] since the self-energy is not included in the present study. Approximately, the self-energy renormalizes the value of  $U_1$  to  $U_1/z$ , where  $z (< 1)$  is the renormalization factor. In order to decide the value of  $U_1$ , we set the value of  $\alpha_s = 0.95$  at  $x = 0$  ( $p_{\text{eff}} = 0.14$ ). The value of  $\alpha_s$  decreases with  $p_{\text{eff}}$ . At  $x = 0.15$  ( $p_{\text{eff}} = 0.24$ ), moderate spin fluctuations,  $\alpha_s = 0.91$ , are obtained. These moder-

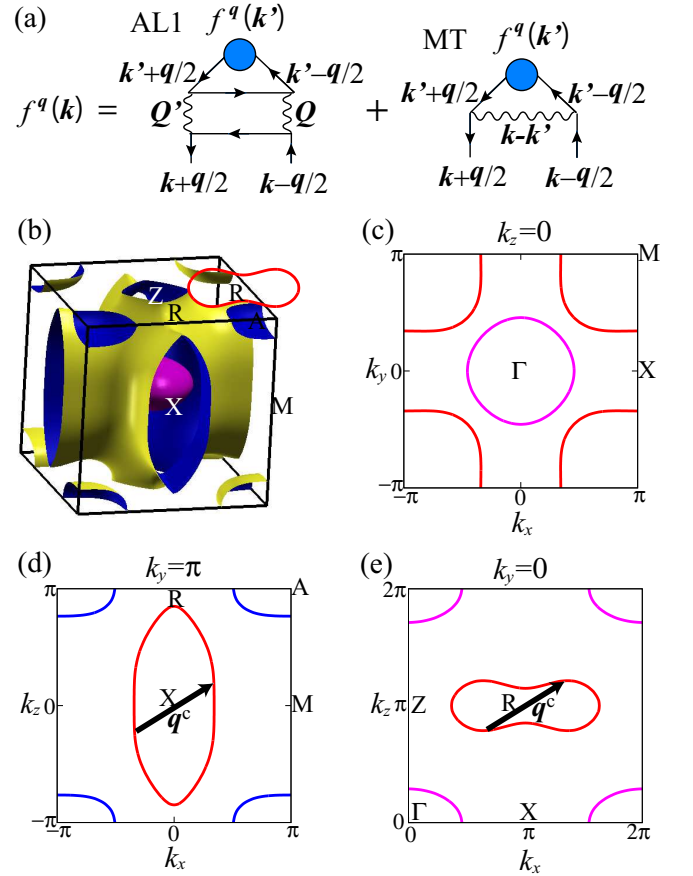


FIG. 1. (a) Feynman diagrams of the AL1 and MT terms in the DW Eq., where the wavy lines represent the spin fluctuations. (b) 3D FSs in the present NdNiO<sub>2</sub> model, where the red line represents FS around the R point shown in Fig. 1 (e). (c) FSs on  $k_z = 0$  plane. (d) FSs on  $k_y = \pi$  plane. (e) FSs on  $k_y = 0$  plane. Red, purple, and blue lines show FSs composed of orbitals 1, 2, and 3, respectively. Black arrows are secondary 3D nesting vector  $\mathbf{q}^c \sim (2\pi/3, 0, q_z^c)$  ( $0.2\pi \lesssim q_z^c \lesssim 2\pi/3$ ).

ate spin fluctuations are consistent with the experiment, where  $1/T_1 T$  moderately increases for  $T \lesssim 100\text{K}$  [62].

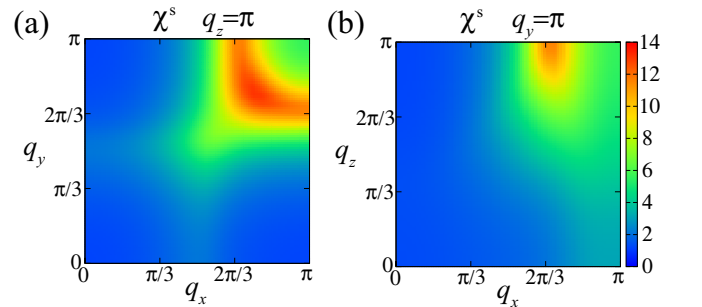


FIG. 2. (a)  $\mathbf{q}$  dependences of  $\chi^s(\mathbf{q}, 0)$  given by the RPA on  $q_z = \pi$  plane, and (b) that on  $q_y = \pi$  plane in NdNiO<sub>2</sub>.

Next, we analyze the CDW state in NdNiO<sub>2</sub> based on

the charge-channel DW equation [44, 46, 58]. A rigorous formalism of the DW equation has been constructed based on the Luttinger–Ward theory in Ref. [63]. The solution of the DW equation gives the minimum of the grand potential in the Luttinger–Ward theory, and therefore it is thermodynamically stable. The optimized non-local form factor  $f^{\mathbf{q}}(k)$  for orbital 1, which describes the DW order parameter, is derived from the following linearized DW equation:

$$\lambda_{\mathbf{q}} f^{\mathbf{q}}(k) = \frac{T}{N} \sum_{k'} I^{\mathbf{q}}(k, k') g^{\mathbf{q}}(k') f^{\mathbf{q}}(k'), \quad (1)$$

$\lambda_{\mathbf{q}}$  is the eigenvalue of the form factor  $f^{\mathbf{q}}(k)$ ,  $g^{\mathbf{q}}(k) \equiv -G(k + \frac{\mathbf{q}}{2}) G(k - \frac{\mathbf{q}}{2})$ ,  $I^{\mathbf{q}}(k, k')$  is the four-point vertex, and  $k = [\mathbf{k}, \epsilon_n = (2n + 1)\pi T]$ . The charge-channel DW with wave vector  $\mathbf{q}$  is established when the largest  $\lambda_{\mathbf{q}} = 1$ . The DW susceptibility is proportional to  $(1 - \lambda_{\mathbf{q}})^{-1}$  [63]. Therefore,  $\lambda_{\mathbf{q}}$  represents the strength of the DW instability. In the DW Eq. (1), the Maki–Thompson (MT) terms and AL terms are included in the four-point vertex, as we explain in SM A [16]. Notably, the bond order solutions in the square lattice and the anisotropic triangular lattice Hubbard models [64] obtained by the DW Eq. have been verified by the renormalization group (RG) methods [53, 56, 57], where the higher-order vertex corrections are generated in a systematic and unbiased manner. When  $\chi^s(\mathbf{q})$  is large, the AL term in Fig. 1(a) is strongly enhanced in proportion to  $\sum_p \chi^s(\mathbf{p} + \mathbf{q}^c/2) \chi^s(\mathbf{p} - \mathbf{q}^c/2)$ , where  $\mathbf{Q} = \mathbf{p} + \mathbf{q}^c/2$  and  $\mathbf{Q}' = \mathbf{p} - \mathbf{q}^c/2$  close to the paramagnon wave vector  $\mathbf{Q}_s$  give dominant contribution. [44, 46]. As a result, the interference mechanism causes the charge-channel DW order at  $\mathbf{q}^c \approx \mathbf{Q} - \mathbf{Q}'$ . The MT term is also important for the  $\mathbf{k}$  dependence of  $f^{\mathbf{q}}(k)$ .

Figures 3(a) and (b) show the  $\mathbf{q}$  dependence of the obtained  $\lambda_{\mathbf{q}}$ , which peaks at the 3D secondary nesting vector  $\mathbf{q}^c$ . From the Fourier transformation of  $f^{\mathbf{q}^c}(\mathbf{k})$  shown in SM B [16], the obtained order is identified as the  $d_{x^2-y^2}$ -wave bond order. The bond order has a period-three modulation in the  $x$ -direction as shown in Fig. 3(c) due to the  $q_x$  component of  $\mathbf{q}^c$  ( $q_x^c \sim 2\pi/3$ ). In the bond-ordered state, the hopping integrals are modulated. The obtained period-three bond order is consistent with the experiments [12–15]. Since  $\mathbf{q}^c$  has  $q_z$  component  $q_z^c$ , the bond order also has a modulation along the  $z$ -direction, which is consistent with the 3D CDW with  $q_z \sim 0.6\pi$  and  $q_z \lesssim 0.54\pi$  observed in Ref. [14].

In the following, we explain the decisive role of the non-locality of the irreducible four-point vertex on the 3D bond order [43–49, 58]. As discussed in Ref. [58], in the presence of moderate spin fluctuations, the AL terms give strong attraction between the Fermi momenta  $\mathbf{k}$  and  $\mathbf{k}' = \pm\mathbf{k}$  in the DW Eq. (1), which leads to the relation  $f^{\mathbf{q}^c}(\mathbf{k}) f^{\mathbf{q}^c}(\mathbf{k}') > 0$  for  $\mathbf{k}' = \pm\mathbf{k}$ . Thus, the AL terms strongly enhance the instability of various even-parity [ $f(\mathbf{k}) = f(-\mathbf{k})$ ] DW states. In addition, the MT term

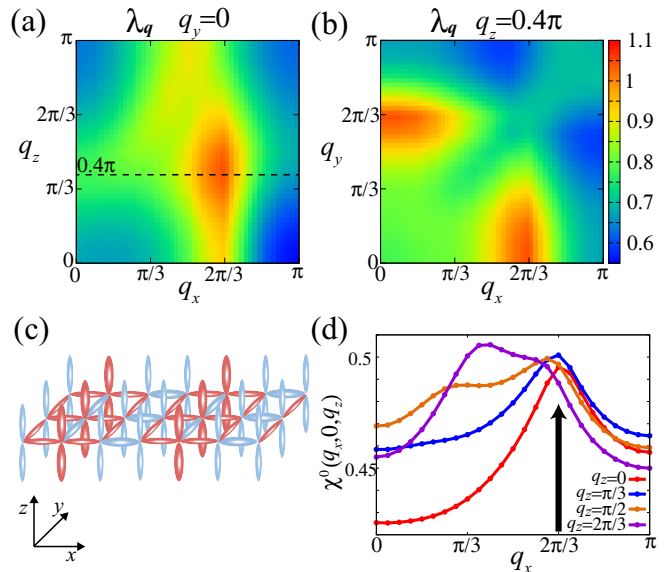


FIG. 3. (a) Obtained  $\mathbf{q}$  dependence of  $\lambda_{\mathbf{q}}$  on  $q_y = 0$  plane, and (b) that on  $q_z = 0.4\pi$  plane. (c) Schematic picture of 3D bond order, where the red and blue bonds denote increased and decreased hoppings. In addition, this bond order also has a modulation along the  $z$ -direction. (d)  $q_x$  dependence of  $\chi^0(q_x, 0, q_z)$  for each  $q_z$  at  $x = 0$ .

in Fig. 1(a) gives moderate repulsion between the Fermi momenta  $\mathbf{k}$  and  $\mathbf{k}' = \mathbf{k} - \mathbf{Q}_s$ , which leads to the relation  $f^{\mathbf{q}^c}(\mathbf{k}) f^{\mathbf{q}^c}(\mathbf{k} - \mathbf{Q}_s) < 0$  at  $\mathbf{Q}_s \sim (2\pi/3, 2\pi/3, \pi)$ . The MT term favors the  $d$ -wave form factor with sign reversal, as shown in Figs. S2(a) and (b) in SM B [16]. Due to the cooperation between the attraction by the AL terms and the repulsion by the MT term, the  $d_{x^2-y^2}$ -wave bond order is naturally realized at high transition temperature. We note that the non-local and non- $s$ -wave DW states cannot be obtained when locally approximated  $\hat{I}_{\text{local}}^{\mathbf{q}}(\epsilon_n, \epsilon_{n'}) = \sum_{\mathbf{k}, \mathbf{k}'} \hat{I}^{\mathbf{q}}(k, k')$  is applied, even if the AL and MT terms are taken into account [64].

Here, we also explain the importance of the secondary 3D nesting with short wavelength shown in Fig. 1(d) and (e). This nesting assists the  $\mathbf{q}^c$  bond order.  $g^{\mathbf{q}}(k)$  in the DW Eq. (1) becomes large when both  $\mathbf{k} + \frac{\mathbf{q}}{2}$  and  $\mathbf{k} - \frac{\mathbf{q}}{2}$  locate on the FSs. The existence of this nesting is well recognized in a broad peak structure of irreducible susceptibilities  $\chi^0(\mathbf{q}) (\propto \sum_{\mathbf{k}} g^{\mathbf{q}}(k))$  for orbital 1 as shown in Fig. 3(d). This secondary nesting stabilizes the 3D CDW in NdNiO<sub>2</sub>.

We stress that the  $\mathbf{q} = \mathbf{0}$  DW orders have been realized in various systems such as cuprates and Fe-based superconductors, and they can be naturally explained by the paramagnon-interference mechanism. The  $\mathbf{q}$  dependence of DW order is sensitive to the structure of FSs. The three-dimensionality in FSs might be important to understand the absence of  $\mathbf{q} = \mathbf{0}$  order. Clarifying the presence or absence of  $\mathbf{q} = \mathbf{0}$  order in  $R\text{NiO}_2$  is an im-

portant future problem.

Here, we discuss the doping  $x$  dependence of the CDW in  $\text{Nd}_{1-x}\text{Sr}_x\text{NiO}_2$ . In this study, the hole-doping  $x$  is introduced by the rigid-band shift for all three bands. Figure 4(a) shows  $x$  dependence of  $q_x^{\text{max}}$ .  $q_x^{\text{max}}$  is defined as  $q_x$  component of  $\mathbf{q}$ , where  $\lambda_{\mathbf{q}}$  becomes maximum. The value of  $q_x^{\text{max}}$  decreases with hole-doping  $x$  since the distance of the two FSs around the M point, which is related to the 3D nesting  $\mathbf{q}^c$ , decreases with  $x$ . This  $x$  dependence is consistent with the experimental results [12].

In order to derive the theoretical transition temperature  $T_c^{\text{DW}}$ , we calculate the  $T$  dependences of the maximum value of  $\lambda_{\mathbf{q}}$  ( $= \lambda_{\text{max}}$ ) and  $\alpha_s$ . As shown in Fig. 4(b),  $\lambda_{\text{max}}$  reaches 1 at  $T_c^{\text{DW}} = 73\text{meV}$  for  $x = 0$  ( $p_{\text{eff}} = 0.14$ ), while the spin-ordered state is absent because  $\alpha_s < 1$ .

As discussed in SM A [16], we confirm that the obtained results for  $T \geq 60\text{meV}$  are reliable. Figure 4(c) shows the obtained  $T$  dependence of  $\lambda_{\text{max}}$  for each  $x$  for  $T \geq 60\text{meV}$ . We obtain almost perfect  $T$ -linear  $\lambda_{\text{max}}$  for all  $x$ , and it reaches unity for  $x < 0.05$ .

The  $T$ -linear  $\lambda_{\mathbf{q}=0}$  is generally realized in the paramagnon-interference mechanism, like Fe-based superconductors [63], which is consistent with the Curie-Weiss behavior of nematic susceptibility observed in experiments [65, 66]. Since the mechanism of the present 3D CDW is the same paramagnon interference, the  $T$ -linear behavior of  $\lambda_{\text{max}}$  is expected. By extrapolating the  $T$ -linear  $\lambda_{\text{max}}$  shown by dotted line, we obtain reliable  $T_c^{\text{DW}} (< 60\text{meV})$  for each  $x \geq 0.05$  shown in Fig. 4(d). This  $x$  dependence of long-range order  $T_c^{\text{DW}}$  is consistent with recent RIXS measurements [12–15, 17, 18].

At the bond-order QCP ( $T_c^{\text{DW}} = 0$ ), the non-Fermi-liquid transport phenomena and the strong pairing interaction are induced by the bond-order fluctuations [60]. In fact, non-Fermi-liquid transport phenomena [19, 20] and the enhancement of  $T_{\text{SC}}$  and  $H_{c2}$  have been observed near the bond-order QCP.

In the present study, the obtained  $q_z^c$  of the 3D CDW is incommensurate. In contrast,  $q_z = 0$  of the 3D CDW has been observed in YBCO cuprates under a large magnetic field and a uniaxial strain [67–71]. This significant difference is understood by the presence or absence of the 3D secondary nesting. We note that the RIXS peak  $q_z \sim \pi$  in the 2D CDW phase in YBCO is much broader along the  $q_z$ -direction than that of  $\text{NdNiO}_2$  [14, 69–71]. This fact means the realization of the 3D CDW in  $\text{NdNiO}_2$ .

Hereafter, we discuss differences in the CDW quantum critical behaviors between  $R\text{NiO}_2$  and cuprates. The CDW in cuprates has been identified as the bond order by the paramagnon-interference mechanism [54–56]. As shown in Fig. S1(c), the CDW instability at a fixed  $p_{\text{eff}}$  in  $R\text{NiO}_2$  is stronger than that in cuprates. These differences are understood by the strength of the Coulomb interaction:  $U_1 = 3.8\text{eV}$  in  $R\text{NiO}_2$  given by the first-principles calculation is larger than  $U_1 = 2.6\text{eV}$  in Hg cuprates [9]. In addition, the 3D bond order in  $R\text{NiO}_2$  is

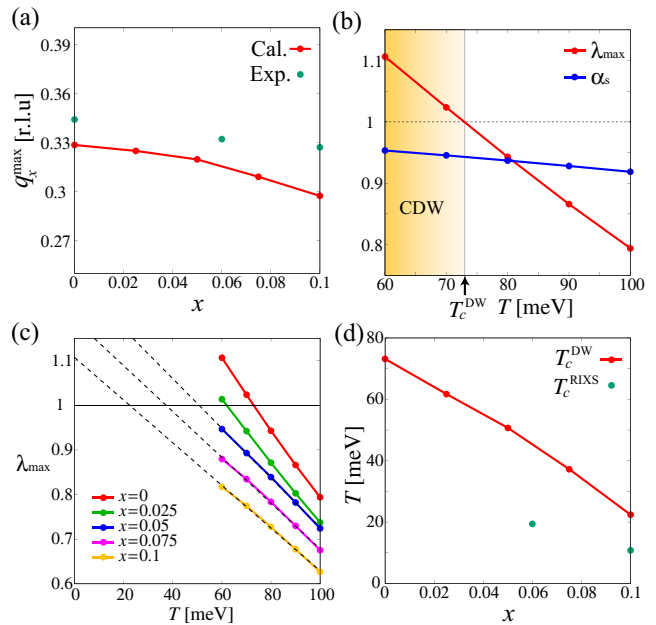


FIG. 4. (a)  $x$  dependences of  $q_x^{\text{max}}$  in  $\text{Nd}_{1-x}\text{Sr}_x\text{NiO}_2$ . (b)  $T$  dependences of  $\lambda_{\text{max}}$  and  $\alpha_s$  for  $x = 0$  ( $p_{\text{eff}} = 0.14$ ). (c) Obtained  $T$  dependences of  $\lambda_{\text{max}}$  for  $x = 0, 0.025, 0.05, 0.075, 0.1$ , where the dotted lines are fitted by the least squares. (d)  $x$  dependences of  $T_c^{\text{DW}}$  and  $T_c^{\text{RIXS}}$ . Lines are calculation results, while green dots represent experimental results in Ref. [12].

stabilized by the 3D nesting  $\mathbf{q}^c$  around R point shown in Fig. 1(e), which is absent in cuprates. For these reasons, the CDW (bond-order) instability in  $R\text{NiO}_2$  is stronger than that in cuprates.

Note that the obtained long-range-order  $T_c^{\text{DW}}$  may be overestimated when the self-energy is not taken into account. In FeSe, the nematic transition temperature  $\sim 100\text{K}$  is well reproduced by introducing the self-energy [63]. Noteworthy, this self-energy suppression is also important in the context of superconducting (SC) fluctuation paraconductivity as discussed in Ref. [72]. Interestingly, the functional RG study [57] revealed that the AL diagrams of SC fluctuations give rise to the orbital order. It is a fruitful future issue to include the SC fluctuations in the kernel function of the DW equation.

In recent years, strong correlation theories such as the DMFT [73–78], the cluster DMFT [79, 80], the 2D density-matrix RG (DMRG) [81–83], and the quantum Monte Carlo methods [80, 84, 85] have made remarkable progress. Mott insulators and pseudogaps can be explained. On the other hand, the DW equation method, which belongs to the weak correlation theory, is suitable for the analysis of “metallic ordered states” such as CDW order [49]. This theory is applicable to various metallic systems, such as “multi-orbital and multi-site models” like iron-based superconductors [43–49], and kagome metals [60]. Notably, both the DW equation method [58] and the DMRG study [86] lead to similar spin current

orders in the square lattice Hubbard model. Thus, the DW equation theory is useful and reliable, and it is complementary to the above strong correlation theories.

In summary, we studied the origin of the 3D CDW in  $RNiO_2$  based on a realistic 3D Hubbard model. We found that the 3D CDW is identified as the  $d$ -wave bond order with the wave vector  $\mathbf{q}^c \sim (2\pi/3, 0, q_z^c)$  ( $0.2\pi \lesssim q_z^c \lesssim 2\pi/3$ ). This 3D bond order with the period-three in the  $x$ -direction as shown in Fig. 3(c) is driven by the paramagnon-interference mechanism, and it is further stabilized by the secondary 3D short-wavelength nesting shown in Figs. 1(e) and (f). The doping dependences of the CDW order have been well reproduced by the present mechanism. The present paramagnon-interference mechanism would be a key concept toward a unified understanding of the CDW orders in nickelates and cuprates. This is an important issue for the future.

We are grateful to Y. Yamakawa for valuable discussions. This work was supported by Grants-in-Aid for Scientific Research from MEXT, Japan (No. JP23H03299, No. JP19H05825, No. JP18H01175, and No. JP17K05543)

- 
- [1] D. Li, K. Lee, B. Y. Wang, M. Osada, S. Crossley, H. R. Lee, Y. Cui, Y. Hikita, and H. Y. Hwang, *Nature* **572**, 624 (2019).
- [2] S. Zeng, C. S. Tang, X. Yin, C. Li, M. Li, Z. Huang, J. Hu, W. Liu, G. J. Omar, H. Jani, Z. S. Lim, K. Han, D. Wan, P. Yang, S. J. Pennycook, A. T. S. Wee, and A. Ariando *Phys. Rev. Lett.* **125**, 147003 (2020).
- [3] M. Osada, B. Y. Wang, B. H. Goodge, K. Lee, H. Yoon, K. Sakuma, D. Li, M. Miura, L. F. Kourkoutis, and H. Y. Hwang, *Nano Lett.* **20**, 5735 (2020).
- [4] N. N. Wang, M. W. Yang, Z. Yang, K. Y. Chen, H. Zhang, Q. H. Zhang, Z. H. Zhu, Y. Uwatoko, L. Gu, X. L. Dong, J. P. Sun, K. J. Jin, and J.-G. Cheng, *Nat. Commun.* **13**, 4367 (2022).
- [5] M. Hepting, D. Li, C. J. Jia, H. Lu, E. Paris, Y. Tseng, X. Feng, M. Osada, E. Been, Y. Hikita, Y.-D. Chuang, Z. Hussain, K. J. Zhou, A. Nag, M. Garcia-Fernandez, M. Rossi, H. Y. Huang, D. J. Huang, Z. X. Shen, T. Schmitt, H. Y. Hwang, B. Moritz, J. Zaanen, T. P. Devereaux and W. S. Lee, *Nat. Mater.* **19**, 381 (2020).
- [6] Y. Nomura, M. Hirayama, T. Tadano, Y. Yoshimoto, K. Nakamura, and R. Arita, *Phys. Rev. B* **100**, 205138 (2019).
- [7] J. Karp, A. S. Botana, M. R. Norman, H. Park, M. Zingl, and A. Millis, *Phys. Rev. X* **10**, 021061 (2020).
- [8] X. Wu, D. DiSante, T. Schwemmer, W. Hanke, H. Y. Hwang, S. Raghu, and R. Thomale, *Phys. Rev. B* **101**, 060504(R) (2020).
- [9] H. Sakakibara, H. Usui, K. Suzuki, T. Kotani, H. Aoki, and K. Kuroki, *Phys. Rev. Lett.* **125**, 077003 (2020).
- [10] R. Zhang, C. Lane, B. Singh, J. Nokelainen, B. Barbiellini, R. S. Markiewicz, A. Bansil, and J. Sun, *Commun. Phys.* **4**, 118 (2021).
- [11] J. Zaanen, G. A. Sawatzky, and J. W. Allen, *Phys. Rev. Lett.* **55**, 418 (1985).
- [12] M. Rossi, M. Osada, J. Choi, S. Agrestini, D. Jost, Y. Lee, H. Lu, B. Y. Wang, K. Lee, A. Nag, Y.-D. Chuang, C.-T. Kuo, S.-J. Lee, B. Moritz, T. P. Devereaux, Z.-X. Shen, J.-S. Lee, K.-J. Zhou, H. Y. Hwang, and W.-S. Lee *Nat. Phys.* **18**, 869 (2022).
- [13] C. C. Tam, J. Choi, X. Ding, S. Agrestini, A. Nag, M. Wu, B. Huang, H. Luo, P. Gao, M. G.-Fernandez, L. Qiao, and K.-J. Zhou, *Nat. Mater.* **21**, 1116 (2022).
- [14] G. Krieger, L. Martinelli, S. Zeng, L. E. Chow, K. Kummer, R. Arpaia, M. Moretti Sala, N. B. Brookes, A. Ariando, N. Viart, M. Salluzzo, G. Ghiringhelli, and D. Preziosi, *Phys. Rev. Lett.* **129**, 027002 (2022).
- [15] X. Ren, R. Sutarto, Q. Gao, Q. Wang, J. Li, Y. Wang, T. Xiang, J. Hu, F. Zhang, J. Chang, R. Comin, X. J. Zhou, and Z. Zhu, arXiv:2303.02865.
- [16] Supplemental Material
- [17] W. Tabis, Y. Li, M. Le Tacon, L. Braicovich, A. Kreyssig, M. Minola, G. Dellea, E. Weschke, M. J. Veit, M. Ramazanoglu, A. I. Goldman, T. Schmitt, G. Ghiringhelli, N. Barišić, M. K. Chan, C. J. Dorow, G. Yu, X. Zhao, B. Keimer, and M. Greven, *Nat. Commun.* **5**, 5875 (2014).
- [18] T. P. Croft, C. Lester, M. S. Senn, A. Bombardi, and S. M. Hayden, *Phys. Rev. B* **89**, 224513 (2014).
- [19] D. Li, B. Y. Wang, K. Lee, S. P. Harvey, M. Osada, B. H. Goodge, L. F. Kourkoutis, and H. Y. Hwang, *Phys. Rev. Lett.* **125**, 027001 (2020).
- [20] K. Lee, B. Y. Wang, M. Osada, B. H. Goodge, T. C. Wang, Y. Lee, S. Harvey, W. J. Kim, Y. Yu, C. Murthy, S. Raghu, L. F. Kourkoutis, H. Y. Hwang, *Nature* **619**, 288 (2023).
- [21] H. Takagi, T. Ido, S. Ishibashi, M. Uota, S. Uchida, and Y. Tokura, *Phys. Rev. B* **40**, 2254 (1989).
- [22] H. Kontani, *Rep. Prog. Phys.* **71**, 026501 (2008).
- [23] Y. Zhong, Y. Wang, S. Han, Y.-F. Lv, W.-L. Wang, D. Zhang, H. Ding, Y.-M. Zhang, L. Wang, K. He, R. Zhong, J. A. Schneeloch, G.-D. Gu, C.-L. Song, X.-C. Ma, and Q.-K. Xue, *Sci. Bull.* **61**, 1239 (2016).
- [24] S.-D. Chen, M. Hashimoto, Y. He, D. Song, K.-J. Xu, J.-F. He, T. P. Devereaux, H. Eisaki, D.-H. Lu, J. Zaanen, and Z.-X. Shen, *Science* **366**, 1099 (2019).
- [25] J.-Q. Fan, X.-Q. Yu, F.-J. Cheng, H. Wang, R. Wang, X. Ma, X.-P. Hu, D. Zhang, X.-C. Ma, Q.-K. Xue, and C.-L. Song, *Natl. Sci. Rev.* **9**, nwab225 (2022).
- [26] H. Chen, Y.-F. Yang, G.-M. Zhang, *Nat. Commun.* **14**, 5477 (2023).
- [27] K. G. Slobodchikov and I. V. Leonov, *Phys. Rev. B* **106**, 165110 (2022).
- [28] E. Fradkin, S. A. Kivelson, and J. M. Tranquada, *Rev. Mod. Phys.* **87**, 457 (2015).
- [29] Y. Wang, D. F. Agterberg, and A. V. Chubukov, *Phys. Rev. Lett.* **114**, 197001 (2015).
- [30] P. A. Lee, *Phys. Rev. X* **4**, 031017 (2014).
- [31] J. C. S. Davis and D.-H. Lee, *Proc. Natl. Acad. Sci. USA* **110**, 17623 (2013).
- [32] R. M. Fernandes, L. H. VanBebber, S. Bhattacharya, P. Chandra, V. Keppens, D. Mandrus, M. A. McGuire, B. C. Sales, A. S. Sefat, and J. Schmalian, *Phys. Rev. Lett.* **105**, 157003 (2010).
- [33] R. M. Fernandes, E. Abrahams, and J. Schmalian, *Phys. Rev. Lett.* **107**, 217002 (2011).
- [34] F. Wang, S. A. Kivelson, and D.-H. Lee, *Nat. Phys.* **11**, 959 (2015).
- [35] R. Yu, and Q. Si, *Phys. Rev. Lett.* **115**, 116401 (2015).

- [36] J. K. Glasbrenner, I. I. Mazin, H. O. Jeschke, P. J. Hirschfeld, and R. Valenti, *Nat. Phys.* **11**, 953 (2015).
- [37] C. Fang, H. Yao, W.-F. Tsai, J. P. Hu, and S. A. Kivelson, *Phys. Rev. B* **77**, 224509 (2008).
- [38] R. M. Fernandes and A. V. Chubukov, *Rep. Prog. Phys.* **80**, 014503 (2017).
- [39] F. Krüger, S. Kumar, J. Zaanen, J. van den Brink, *Phys. Rev. B* **79**, 054504 (2009).
- [40] W. Lv, J. Wu, and P. Phillips, *Phys. Rev. B* **80**, 224506 (2009).
- [41] C.-C. Lee, W.-G. Yin, and W. Ku, *Phys. Rev. Lett.* **103**, 267001 (2009).
- [42] H. Kontani and S. Onari, *Phys. Rev. Lett.* **104**, 157001 (2010).
- [43] S. Onari and H. Kontani, *Phys. Rev. Lett.* **109**, 137001 (2012).
- [44] S. Onari, Y. Yamakawa, and H. Kontani, *Phys. Rev. Lett.* **116**, 227001 (2016).
- [45] Y. Yamakawa, S. Onari and H. Kontani, *Phys. Rev. X* **6**, 021032 (2016).
- [46] S. Onari and H. Kontani, *Phys. Rev. B* **100**, 020507(R) (2019).
- [47] S. Onari and H. Kontani, *Phys. Rev. Research* **2**, 042005(R) (2020).
- [48] S. Onari and H. Kontani, *Front. Phys.* **10**, 915619 (2022).
- [49] H. Kontani, R. Tazai, Y. Yamakawa, and S. Onari, *Adv. Phys.* DOI:10.1080/00018732.2022.2144590.
- [50] K. Jiang, J. Hu, H. Ding, and Z. Wang, *Phys. Rev. B* **93**, 115138 (2016).
- [51] L. Fanfarillo, G. Giovannetti, M. Capone, and E. Bascones, *Phys. Rev. B* **95**, 144511 (2017).
- [52] R. Q. Xing, L. Classen, A. V. Chubukov, *Phys. Rev. B* **98**, 041108(R) (2018).
- [53] A. V. Chubukov, M. Khodas, and R. M. Fernandes, *Phys. Rev. X* **6**, 041045 (2016).
- [54] Y. Yamakawa and H. Kontani, *Phys. Rev. Lett.* **114**, 257001 (2015).
- [55] K. Kawaguchi, M. Tsuchiizu, Y. Yamakawa, and H. Kontani, *J. Phys. Soc. Jpn.* **86**, 063707 (2017).
- [56] M. Tsuchiizu, K. Kawaguchi, Y. Yamakawa, and H. Kontani, *Phys. Rev. B* **97**, 165131 (2018).
- [57] M. Tsuchiizu, Y. Ohno, S. Onari, and H. Kontani, *Phys. Rev. Lett.* **111**, 057003 (2013).
- [58] H. Kontani, Y. Yamakawa, R. Tazai, and S. Onari, *Phys. Rev. Research* **3**, 013127 (2021).
- [59] S. Onari and H. Kontani, *Phys. Rev. Lett.* **128**, 066401 (2022).
- [60] R. Tazai, Y. Yamakawa, S. Onari, and H. Kontani, *Sci. Adv.* **8**, eabl4108 (2022).
- [61] R. Tazai, Y. Yamakawa, and H. Kontani, *Nat. Commun.* **14**, 7845 (2023).
- [62] Y. Cui, C. Li, Q. Li, X. Zhu, Z. Hu, Y.-F. Yang, J. Zhang, R. Yu, H.-H. Wen, and W. Yu, *Chin. Phys. Lett.* **38**, 067401 (2021).
- [63] R. Tazai, S. Matsubara, Y. Yamakawa, S. Onari, and H. Kontani, *Phys. Rev. B* **107**, 035137 (2023).
- [64] R. Tazai, Y. Yamakawa, M. Tsuchiizu, and H. Kontani, *J. Phys. Soc. Jpn.* **86**, 073703 (2017).
- [65] J. H. Chu, H. H. Kuo, J. G. Analytis, I. R. Fisher, *Science* **337**, 710 (2012).
- [66] A. E. Böhrmer, P. Burger, F. Hardy, T. Wolf, P. Schweiss, R. Fromknecht, M. Reinecker, W. Schranz, and C. Meingast, *Phys. Rev. Lett.* **112**, 047001 (2014).
- [67] T. Wu, H. Mayaffre, S. Krämer, M. Horvatić, C. Berthier, W. N. Hardy, R. Liang, D. A. Bonn, and M.-H. Julien, *Nature* **477**, 191 (2011).
- [68] B. Keimer, S. A. Kivelson, M. R. Norman, S. Uchida, and J. Zaanen, *Nature* **518**, 179 (2015).
- [69] S. Gerber, H. Jang, H. Nojiri, S. Matsuzawa, H. Yasumura, D. A. Bonn, R. Liang, W. N. Hardy, Z. Islam, A. Mehta, S. Song, M. Sikorski, D. Stefanescu, Y. Feng, S. A. Kivelson, T. P. Devereaux, Z.-X. Shen, C.-C. Kao, W.-S. Lee, D. Zhu, J.-S. Lee, *Science* **350**, 949 (2015).
- [70] J. Chang, E. Blackburn, O. Ivashko, A. T. Holmes, N. B. Christensen, M. Hücker, R. Liang, D. A. Bonn, W. N. Hardy, U. Rütt, M. v. Zimmermann, E. M. Forgan, and S. M. Hayden, *Nat. Commun.* **7**, 11494 (2016).
- [71] H.-H. Kim, E. Lefrancois, K. Kummer, R. Fumagalli, N. B. Brookes, D. Betto, S. Nakata, M. Tortora, J. Porras, T. Loew, M. E. Barber, L. Braicovich, A.P. Mackenzie, C. W. Hicks, B. Keimer, M. Minola, M. Le Tacon, *Phys. Rev. Lett.* **126**, 037002 (2021).
- [72] V. Dorin, R. A. Klemm, A. A. Varlamov, A. I. Buzdin, and D. V. Livanov, *Phys. Rev. B* **48**, 12951 (1993).
- [73] W. Metzner and D. Vollhardt, *Phys. Rev. Lett.* **62**, 324 (1989).
- [74] M. Jarrell, *Phys. Rev. Lett.* **69**, 168 (1992).
- [75] A. Georges and W. Krauth, *Phys. Rev. Lett.* **69**, 1240 (1992).
- [76] A. Georges, G. Kotliar, W. Krauth, and M. J. Rozenberg, *Rev. Mod. Phys.* **68**, 13 (1996).
- [77] A. Liebsch, H. Ishida, and J. Merino, *Phys. Rev. B* **78**, 165123 (2008).
- [78] S. Shiro, *J. Phys. Soc. Jpn.* **92**, 092001 (2023).
- [79] T. A. Maier, M. Jarrell, T. Pruschke, and M. Hettler, *Rev. Mod. Phys.* **77**, 1027 (2005).
- [80] T. Schäfer *et al.*, *Phys. Rev. X* **11**, 011058 (2021).
- [81] S. R. White, *Phys. Rev. Lett.* **69**, 2863 (1992)
- [82] E. M. Stoudenmire and S. R. White, *Annu. Rev. Condens. Matter Phys.* **3**, 111 (2012).
- [83] J. P. F. LeBlanc *et al.*, *Phys. Rev. X* **5**, 041041 (2015).
- [84] N. V. Prokofev and B. V. Svistunov, *Phys. Rev. Lett.* **81**, 2514 (1998).
- [85] R. Blankenbecler, D. J. Scalapino, and R. L. Sugar, *Phys. Rev. D* **24**, 2278 (1981).
- [86] K. Shinjo, S. Sota, S. Yunoki, T. Tohyama, *Phys. Rev. B* **108**, 195118 (2023).

[Supplementary Material]  
**Three-dimensional bond-order instability in infinite-layer nickelates due to nonlocal quantum interference**

Seiichiro Onari and Hiroshi Kontani

*Department of Physics, Nagoya University, Nagoya 464-8602, Japan*

**A: Model Hamiltonian of NdNiO<sub>2</sub>, formalism of the RPA and the DW equation**

First, we introduce a tight-binding model for NdNiO<sub>2</sub> by referring the tight-binding model in Ref. [1]. We modify the hoppings of Ni  $d_{x^2-y^2}$  orbital in order to reproduce the parallel FSs around the M point, which have been obtained in other first-principles calculations [2, 3]. We modify the intralayer next-nearest-neighbor hopping  $t_2$ , the intralayer third-nearest one  $t_3$ , interlayer nearest one  $t_z$ , and next-nearest-interlayer one  $t_{z2}$  to  $t_2/t_1 = -1/3$ ,  $t_3/t_1 = 0.2$ ,  $t_z/t_1 = 2/3$ , and  $t_{z2}/t_1 = -0.165$  ( $t_1$  is the nearest-neighbor hopping), respectively. These intralayer hoppings are similar to those in YBCO cuprate. The obtained band dispersion is shown in Fig. S1(a).

Here, we explain the Coulomb interaction introduced in the present study. Ni  $d_{x^2-y^2}$  orbital, Nd  $d_{z^2}$  orbital, and Nd  $d_{xy}$  orbital are included in our model. We introduced the on-site Coulomb interaction  $U_1$  for Ni  $d_{x^2-y^2}$  orbital. By using the Coulomb interaction, the spin (charge) susceptibility for orbital 1 in the RPA is given by

$$\chi^{s(c)}(q) = \chi^0(q)[1 - (+)U_1\chi^0(q)]^{-1}, \quad (\text{S1})$$

where the irreducible susceptibility is

$$\chi^0(q) = -\frac{T}{N} \sum_{\mathbf{k}} G(\mathbf{k} + \mathbf{q})G(\mathbf{k}). \quad (\text{S2})$$

$G(\mathbf{k})$  is the Green function for orbital 1 without self-energy  $G(\mathbf{k}) = [\frac{1}{(i\epsilon_n - \mu)\mathbb{1} - \hat{h}^0(\mathbf{k})}]_{1,1}$  for  $\mathbf{k} = [\mathbf{k}, \epsilon_n = (2n + 1)\pi T]$ . Here,  $\hat{h}^0(\mathbf{k})$  is the matrix expression of  $H^0$  and  $\mu$  is the chemical potential.

In the present study, we set  $U_1 = 1.43\text{eV}$ . We use  $N = N_{\mathbf{k}}^3 = 48 \times 48 \times 48$   $\mathbf{k}$  meshes and  $N_{\omega} = 4096$  Matsubara frequencies.

The four-point vertex  $I^{\mathbf{q}}(k, k')$  for orbital 1 in the DW Eq. (1) is given as

$$I^{\mathbf{q}}(k, k') = \sum_{b=s,c} \left[ -\frac{a^b}{2} V^b(k - k') \right. \\ \left. + \frac{T}{N} \sum_p \frac{a^b}{2} V^b\left(p + \frac{\mathbf{q}}{2}\right) V^b\left(p - \frac{\mathbf{q}}{2}\right) \right. \\ \left. \times G(k - p)G(k' - p) \right]$$

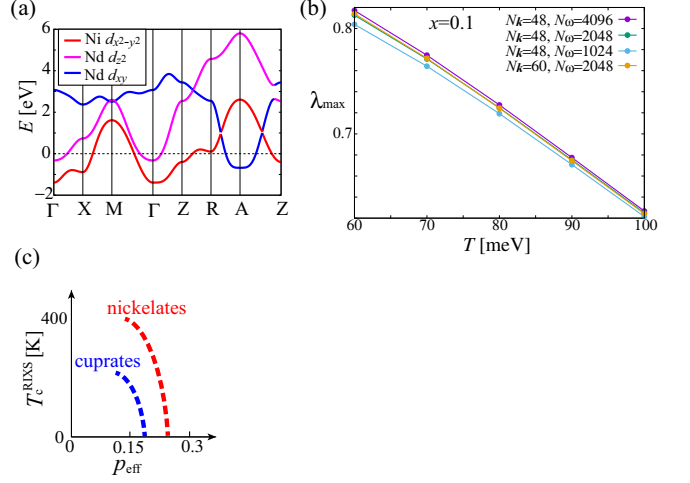


FIG. S1. (a) Band dispersion of NdNiO<sub>2</sub>. (b)  $T$  dependences of  $\lambda_{\max}$  at  $x = 0.1$  for several  $N_{\mathbf{k}}$  and  $N_{\omega}$ . (c) Schematic  $p_{\text{eff}}$  dependences of  $T_c^{\text{RIXS}}$  in nickelates and overdoped cuprates.

$$+ \frac{T}{N} \sum_p \frac{a^b}{2} V^b\left(p + \frac{\mathbf{q}}{2}\right) V^b\left(p - \frac{\mathbf{q}}{2}\right) \\ \times G(k - p)G(k' + p)], \quad (\text{S3})$$

where  $a^s = 3$ ,  $a^c = 1$ ,  $p = (\mathbf{p}, \omega_l)$ , and  $V^{s(c)}(q) = +(-)U_1 + U_1^2 \chi^{s(c)}(q)$ .  $\mathbf{Q}$  and  $\mathbf{Q}'$  in Fig. 1 (a) are given by  $\mathbf{Q} = \mathbf{p} + \mathbf{q}/2$  and  $\mathbf{Q}' = \mathbf{p} - \mathbf{q}/2$ .

In Eq. (S3), the first line corresponds to the MT term, and the second and third lines give the AL1 and AL2 terms, respectively. In the MT term, the first-order term with respect to  $U_1$  gives the Hartree-Fock term in the mean-field theory.

Here, the number of Matsubara frequencies  $N_{\omega} = 4096$  is sufficient for  $T \geq 60\text{meV}$  because of the relation  $2\pi T N_{\omega} \gtrsim 100W_{\text{band}} \sim 400\text{eV}$ . However, due to the lack of  $\mathbf{k}$  meshes  $N = N_{\mathbf{k}}^3 = 48 \times 48 \times 48$ , the obtained  $\lambda_{\max}$  would be underestimated at low temperatures. To verify the numerical accuracy for  $T \geq 60\text{meV}$ , we show the  $T$  dependence of  $\lambda_{\max}$  at  $x = 0.1$  for each  $N_{\mathbf{k}} = 48 \sim 60$  and  $N_{\omega} = 1024 \sim 4096$  in Fig. S1(b).

Figure S1(c) shows schematic  $p_{\text{eff}}$  dependences of  $T_c^{\text{RIXS}}$  observed in nickelates and overdoped cuprates.  $T_c^{\text{RIXS}} \lesssim 400\text{K}$  in nickelates is higher than  $T_c^{\text{RIXS}} \lesssim 200\text{K}$  in cuprates.

### B: Detailed results of the form factor

Here, we explain details of the obtained  $\mathbf{q}^c = (2\pi/3, 0, 0.4\pi)$  form factor. Figure S2(a) and (b) show the form factors  $f^{\mathbf{q}^c}(\mathbf{k})$  for orbital 1, which is derived from  $f^{\mathbf{q}^c}(k)$ .  $f^{\mathbf{q}^c}(\mathbf{k})$  is obtained by simple extrapolation of the lowest Matsubara frequency component and the second lowest one. The obtained  $f^{\mathbf{q}^c}(\mathbf{k})$  is not sensitive to the method of analytical connection, which is verified by the results of the Pade approximation. FSs shifted by  $\pm \frac{\mathbf{q}^c}{2}$  are shown by green and orange lines. The form factor has a large value at  $\mathbf{k}$ , where the two shifted FSs overlap since the  $g^{\mathbf{q}^c}(k')$  in the kernel function is enlarged there. The sign change of  $f^{\mathbf{q}^c}(k)$  is induced by the MT term,  $f^{\mathbf{q}^c}(\mathbf{k})f^{\mathbf{q}^c}(\mathbf{k} - \mathbf{Q}_s) < 0$  [ $\mathbf{k} \sim (2\pi/3, 0, \pi)$ ,  $\mathbf{Q}_s \sim (2\pi/3, 2\pi/3, \pi)$ ]. From the  $\mathbf{k}$  dependence of the form factor, we find that the form factor corresponds to the  $d_{x^2-y^2}$ -wave bond order.

In order to study the real space structure of the bond order, we calculate a Fourier transformed form factor  $\tilde{f}(\mathbf{r})$  given as

$$\tilde{f}(\mathbf{r}) = \sum_{\mathbf{k}} f^{\mathbf{q}^c}(\mathbf{k}) e^{-i\mathbf{k}\cdot\mathbf{r}}. \quad (\text{S4})$$

The obtained  $\tilde{f}(\mathbf{r})$  is shown in Figs. S2(c) and (d). The values at the nearest neighbors from  $\mathbf{r} = \mathbf{0}$  are dominant. Sign of  $\tilde{f}(\pm 1, 0, 0)$  is opposite to that of  $\tilde{f}(0, \pm 1, 0)$ , which

means the  $d_{x^2-y^2}$ -wave bond order in  $xy$  plane. Since the magnitude of  $\tilde{f}(0, 0, \pm 1)$  along  $z$ -direction is similar to that of  $\tilde{f}(\pm 1, 0, 0)$ , the bond order has 3D structure. In addition, the small value of  $\tilde{f}(\mathbf{0}) \neq 0$  means emergence of the slight charge order.

The modulation of hopping  $\delta t_{i,j}$  is given by

$$\delta t_{i,j} = 2\tilde{f}(\mathbf{r}_i - \mathbf{r}_j) \cos \left[ \frac{\mathbf{q}^c}{2} \cdot (\mathbf{r}_i + \mathbf{r}_j) \right]. \quad (\text{S5})$$

The obtained period-three  $\delta t_{i,j}$  bond order around  $z = 0$  plane is shown in Fig. 3(c). Since  $\mathbf{q}^c$  has  $q_z$  component  $0.2\pi \lesssim q_z \lesssim 2\pi/3$ , the bond order also modulates along the  $z$ -direction.

- 
- [1] X. Wu, D. D. Sante, T. Schwemmer, W. Hanke, H. Y. Hwang, S. Raghu, and R. Thomale, Phys. Rev. B **101**, 060504(R) (2020).
  - [2] H. Sakakibara, H. Usui, K. Suzuki, T. Kotani, H. Aoki, and K. Kuroki, Phys. Rev. Lett. **125**, 077003 (2020).
  - [3] R. Zhang, C. Lane, B. Singh, J. Nokelainen, B. Barbiellini, R. S. Markiewicz, A. Bansil, and J. Sun, Commun. Phys. **4**, 118 (2021).
  - [4] Y. Nomura, M. Hirayama, T. Tadano, Y. Yoshimoto, K. Nakamura, and R. Arita, Phys. Rev. B **100**, 205138 (2019).



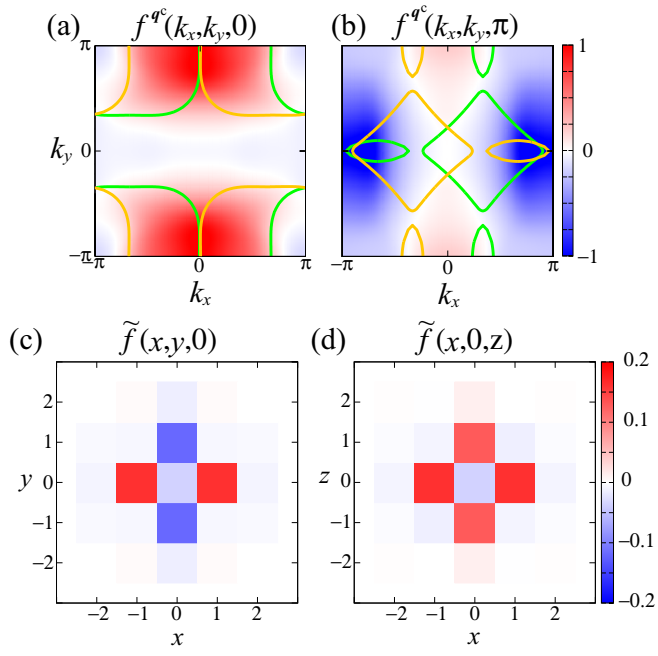


FIG. S2. (a)  $\mathbf{k}$  dependence of  $f^{\mathbf{q}^c}(\mathbf{k})$  for  $\mathbf{q}^c = (2\pi/3, 0, 0.4\pi)$  at  $k_z = 0$  plane, and (b) that at  $k_z = \pi$  plane, where green and orange lines denote FSs shifted by  $\mathbf{q}^c/2$  and  $-\mathbf{q}^c/2$ , respectively. (c)  $\mathbf{r}$  dependence of  $\tilde{f}(\mathbf{r})$  at  $z = 0$  plane, and (d) that at  $y = 0$  plane.